Localized spin-wave modes and microwave absorption in random-anisotropy ferromagnets

Dmitry A. Garanin⬤ and Eugene M. Chudnovsky⬤

Physics Department, Herbert H. Lehman College and Graduate School, The City University of New York,
250 Bedford Park Boulevard West, Bronx, New York 10468-1589, USA

The theory of localized spin-wave excitations in random-anisotropy magnets has been developed. Starting with a pure Heisenberg ferromagnet, we study the evolution of standing spin waves in a finite-size sample towards localized modes on increasing the strength of random anisotropy. Profiles of the localized modes and their phases are analyzed and visualized in a two-dimensional sample. Localization length is obtained by several methods and its dependence on random anisotropy is computed. The connection between the localization of spin excitations and the broadband nature of the absorption of microwave power by random-anisotropy magnets is elucidated.

I. INTRODUCTION

Ferromagnetic exchange, magnetic anisotropy, and dipole-dipole forces are leading interactions that determine the properties of ferromagnets at different spatial scales. At the shortest scales, the exchange, which is usually the strongest interaction, aligns the neighboring spins in one direction. That direction is determined by the magnetic anisotropy due to the symmetry of the underlying crystal lattice. At the largest scale, the dipole-dipole interaction breaks the system into magnetic domains. A less trivial situation occurs in amorphous and sintered ferromagnets where the directions of local magnetic anisotropy axes are random. They exhibit glassy properties that have been intensively studied over the last 50 years, see, e.g., Ref. [1] and references therein. Like for spin glasses, the ground state of random-anisotropy (RA) magnets remains the subject of discussions and controversies. Since seminal works of Larkin [2] and Imry and Ma [3] it has been clear, however, that random pushes of the magnetization by the RA must lead to a significant disordering on a scale that is inversely proportional to some power of the RA strength.

Somewhat less attention has been paid to spin excitations in the RA magnets. In conventional ferromagnets with uniform magnetization, the ac magnetic field can generate uniform ferromagnetic resonance (FMR) and spin waves with a finite wavelength. When the RA magnet is placed in a strong polarizing magnetic field, similar phenomena can occur [4], although the effect of disorder shows in the FMR width and the damping of spin waves. The least understood case, which is of the greatest interest for applications, is the one without the polarizing field when the magnet is fully disordered.

Anderson localization of spin waves due to random anisotropy [5,6] and, more generally, localization of Bose excitations in disordered systems [7–10] has been studied in the past. The effect of randomly distributed lattice defects on the localization of spin waves and magnonic transport has been addressed in Ref. [11]. Experimental evidence of spin-wave localization was reported in amorphous [12–15] and inhomogeneous [16] magnetic films, as well as in heterostructures

[17] and in films with the inhomogeneous magnetic field created by a force microscope [18].

The RA model assumes (see, e.g., Refs. [1,19–21] and references therein) that spins interact via ferromagnetic exchange but that directions of local magnetic anisotropy axes are randomly distributed from one spin to another. When no material anisotropy is introduced by the manufacturing process, an amorphous or sintered magnet has no preference for the orientation of its magnetic moment. Weak local RA cannot break the local ferromagnetic order but it makes the vector of the magnetization wander around the magnet. This model was successfully applied to the description of static properties of amorphous magnets, such as the ferromagnetic correlation length, zero-field susceptibility, the approach to saturation, etc. [22,23]. It was shown that the presence of topological defects makes properties of the model depend on the dimensionality of space: $d = 1$ (thin wires), $d = 2$ (thin films), $d = 3$ (bulk systems), and on the number of spin components (XY model vs Heisenberg) [24].

In recent years, significant attention, driven by applications, has been paid to the absorption of microwaves by nanocomposites made of magnetic particles of various shapes and sizes, see, e.g., Ref. [25] and references therein. Amorphous and sintered ferromagnets represent the ultimate limit of densely packed nanoparticles with distributed properties. In a recent paper [26] we demonstrated that they provide strong broadband absorption of microwave radiation. Evidence has been obtained that it occurs via the absorption of the energy of the ac magnetic field by localized spin excitations.

In this paper, we present a detailed study of such excitations and their effect on microwave power absorption using advantages offered by modern computer power that had not existed when the localization of spin waves in RA ferromagnets was studied before. Instead of preselecting the mechanism of Anderson localization via phase-coherent scattering of spin waves [27], we begin with exciting standing spin waves in a two-dimensional (2D) sample containing 10^4–10^6 spins, and then compute their evolution at finite temperature towards localized oscillations on increasing the strength of the RA. Since the effects we are considering occur on a

spatial scale that is typically small compared with the scale dominated by magnetic dipolar forces, interactions included in our model are ferromagnetic exchange, random magnetic anisotropy, and Zeeman interaction of spins with the ac magnetic field. Our choice of the 2D system is determined by applications of thin films as microwave absorbers.

Classical spin waves in conventional ferromagnets are described by classical Landau-Lifshitz equations and quantized Hamiltonians equally well if their wavelength is large compared to the lattice spacing. It is related to the fact that spins in the commutation relation $[\mathbf{S}_i, \mathbf{S}_j] = i\hbar\epsilon_{ijk}S_k$ almost commute when they describe the coherent motion of groups of spins corresponding to $S \gg 1$. This applies to RA ferromagnets when the ferromagnetic correlation length and the localization length of spin excitations include at least several atomic spins. It is the limit we are considering in this paper, which allows us to neglect quantum effects.

The paper is organized as follows. The model, the numerical method, the description of excitation modes, and the formulas for the power absorption are introduced in Sec. II. Equations describing the time evolution of the excitation modes are derived in Sec. III. Numerical results on visualization of spin excitations in the RA magnet, on the localization transition, phases of the localized modes, are presented in Sec. IV. A separate edge pumping experiment is presented in Sec. V. Brief review of the results and remarks on their relevance to experiments are given in Sec. VI.

II. MODEL, NUMERICAL METHOD, AND EXCITATION MODES

We consider a model of classical spin vectors $\mathbf{s}_i$ ($|\mathbf{s}_i| = 1$) on a square lattice

$$\mathcal{H} = -\frac{1}{2}\sum_{ij}J_{ij}\mathbf{s}_i \cdot \mathbf{s}_j - \frac{D_R}{2}\sum_i(\mathbf{n}_i \cdot \mathbf{s}_i)^2 - \mathbf{H} \cdot \sum_i \mathbf{s}_i, \quad (1)$$

where J_{ij} is the nearest-neighbors exchange interaction with the coupling constant $J > 0$, D_R is the strength of the random anisotropy, $\mathbf{n}_i$ are randomly directed unit vectors, and $\mathbf{H}$ is the magnetic field. The dynamics of classical spins is governed by the Landau-Lifshitz (LL) equation

$$\hbar\dot{\mathbf{s}}_i = \mathbf{s}_i \times \mathbf{H}_{\text{eff},i} - \alpha\mathbf{s}_i \times (\mathbf{s}_i \times \mathbf{H}_{\text{eff},i}), \quad \mathbf{H}_{\text{eff},i} \equiv -\frac{\partial\mathcal{H}}{\partial\mathbf{s}_i}, \quad (2)$$

where $\alpha \ll 1$ is the phenomenological damping constant due to interaction of spins with electrons, phonons, etc. In the subsequent computations, we set $\alpha = 0$ as in the presence of RA and at nonzero temperatures there is an intrinsic damping due to mode hybridization and nonlinearity in the system.

Numerical investigation of the localization of modes is performed in several steps. First, a local energy minimum is found by the energy minimization starting from a collinear or random state of the spins—collinear initial condition (CIC) or random initial condition (RIC). The numerical method [28] combines sequential alignment of spins $\mathbf{s}_i$ with the direction of the local effective field, $\mathbf{H}_{\text{eff},i}$, with the probability η, and the energy-conserving spin flips (over-relaxation), $\mathbf{s}_i \rightarrow 2(\mathbf{s}_i \cdot \mathbf{H}_{\text{eff},i})\mathbf{H}_{\text{eff},i}/H_{\text{eff},i}^2 - \mathbf{s}_i$, with the probability $1 - \eta$. For the pure model, $D_R = 0$, we used $\eta = 0.03$ that ensures the

fastest relaxation. In the presence of RA over-relaxation leads to the energy decrease since the effective field depends on the spin orientation. One can show that flipping of a spin i changes the energy by

$$\Delta E_i = -\frac{D_R}{2}(\Delta\mathbf{s}_i \cdot \mathbf{n}_i)^2, \quad (3)$$

where $\Delta\mathbf{s}_i$ is the change of the spin vector $\mathbf{s}_i$ as the result of the transformation above. Thus for $D_R > 0$ one can use $\eta = 0$ that leads to a relaxation much faster and deeper in the energy than the pure spin alignment, $\eta = 1$. Still, we used $\eta = 0.03$ in all cases.

In the RA system, there are many local energy minima, and the result depends on the initial state. Starting with the collinear state, one arrives at more ordered states than starting from the random spin state. The more ordered state means a higher magnetization $m \equiv |\mathbf{m}|$, where

$$\mathbf{m} = \frac{1}{N}\sum_i \mathbf{s}_i \quad (4)$$

is the average spin and N is the number of spins in the system. Using the Imry-Ma argument, one can estimate that spins are strongly correlated within large regions of the characteristic size R_f (ferromagnetic correlation radius) defined by

$$\frac{R_f}{a} \sim \left(\frac{J}{D_R}\right)^{2/(4-d)}, \quad (5)$$

where a is the lattice spacing and d is the dimensionality of the space, here $d = 2$. In the case $L \gg R_f$, where L is the linear system's size, starting from RIC one arrives at an almost fully disordered state, $m \ll 1$.

Starting from a random initial condition, one obtains spin states with a very small magnetization that decreases with the system size. However, starting from CIC one obtains a state with a significant residual magnetization m in spite of disordering due to RA. As D_R increases from zero, the system quickly disorders down to $m \approx 0.7$ and remains approximately constant up to $D_R/J \approx 5$. Then with a further increase of D_R it gradually decreases down to $m = 0.5$ that corresponds to all spins directed along their local anisotropy axes within a hemisphere. We denote the spin state resulting from energy minimization as $\mathbf{s}_i^{(0)}$ and will use it to study the dynamics of the deviations from this state in the localized modes.

The second step is performing the Metropolis Monte Carlo process at some temperature T to obtain a thermalized state. We are especially interested in very low temperatures, such as $T/J = 0.01$, for which the thermalized state is close to the local-energy-minimum state found in the first step. It is well known that combining Monte Carlo with over-relaxation is very efficient and leads to much faster thermalization than pure Monte Carlo. However, in the presence of RA over-relaxation does not work as it does not conserve the energy, see Eq. (3). Here, over-relaxation can be replaced by the thermalized over-relaxation [1] including spin flips over the part of the effective field that does not include single-site interactions such as RA and accepting or rejecting them with the use of the Metropolis criterion such as in the Monte Carlo routine, whereas the energy change arises because of the single-site interactions. The thermodynamic consistency

of this method has been checked by computing the dynamical spin temperature T_S given by Eq. (9) of Ref. [29]. The values of T_S are in a good accordance with the set temperature T.

The third and most demanding step is to run the dynamical evolution of the system by solving the dissipationless LL equation of motion, Eq. (2) with $\alpha = 0$, in a long time interval. We are using the Butcher's fifth-order Runge-Kutta method, RK5 (see the code, e.g., in the Appendix of Ref. [30]).

We consider the system with free boundary conditions (FBC) for which the SW eigenstates have the factorized form [31]

$$F_{\mathbf{k}i} = f_{n_x k_x} \times f_{n_y k_y}, \tag{6}$$

where the site index i is represented as $i = (n_x, n_y)$ with $n_x = 1, 2, \ldots, N_x$, $n_y = 1, 2, \ldots, N_y$, and $N_x N_y = N$ for the rectangular-shape system. The f functions have the form of standing waves

$$f_{n_\alpha k_\alpha} = \sqrt{\frac{2}{1 + \delta_{k_\alpha 0}}} \cos\left[\left(n_\alpha - \frac{1}{2}\right) a k_\alpha\right], \tag{7}$$

where $\alpha = x, y$ and $a k_\alpha = \pi n_{k_\alpha}/N_\alpha$ with $n_{k_\alpha} = 0, 1, \ldots, N_\alpha - 1$. For a comparison, in a system with periodic boundary conditions (PBC) the eigenstates are $e^{i\mathbf{k}\cdot\mathbf{r}}$ and the wave vectors are quantized as $a k_\alpha = 2\pi n_{k_\alpha}/N_\alpha$ with $n_{k_\alpha} = 0, 1, \ldots, N_\alpha - 1$. This difference is, in fact, arising because of the degeneracy of the wave vectors with respect to their directions in the PBC model that makes the Brillouin zone larger and the values of $\mathbf{k}$ rarified in comparison to the FBC model. For large N the FBC model is closer to the continuous limit than the PBC model. The amplitudes of standing waves $\mathbf{A_k}$ can be computed as the projection of the spin state $\mathbf{s}_{n_x n_y}$ on the eigenfunctions set as

$$\mathbf{A_k}(t) = \frac{1}{N} \sum_{n_x n_y} \mathbf{s}_{n_x n_y}(t) f_{n_x k_x} f_{n_y k_y}.. \tag{8}$$

For $D_R = 0$ and very low temperatures, transverse correlation functions $G_{tr,k}(t)$ are pure sinusoidals with the frequencies

$$\hbar \omega_{\mathbf{k}} = 4J\left\{1 - \frac{1}{2}[\cos(a k_y) + \cos(a k_y)]\right\}. \tag{9}$$

However, at nonzero temperatures they become damped because of spin-wave processes and at elevated temperatures they become overdamped. Random anisotropy causes damping of spin waves in the whole temperature range. If RA is strong enough, SW become overdamped and the description of the system's excitation modes in terms of the sinusoidal waves with a particular wave vectors becomes inadequate. In this case, excitation modes become localized.

To study extended and localized modes, we use the following way of processing the dynamical evolution result $\mathbf{s}_i(t)$. For a very low temperature, such as $T/J = 0.01$, we perform a Fourier transformation of the deviation of the spins from the local energy-minimum state, $\delta\mathbf{s}_i(t) \equiv \mathbf{s}_i(t) - \mathbf{s}_i^{(0)}$ with a set of frequencies, say, the frequencies given by Eq. (9) for the chosen set of $\mathbf{k}$:

$$\delta\tilde{\mathbf{s}}_i(\omega) = \frac{1}{\sqrt{t}} \int_0^t dt' e^{i\omega t'} \delta\mathbf{s}_i(t'). \tag{10}$$

The spin deviations $\delta\mathbf{s}_i$ are expected to precess around $\mathbf{s}_i^{(0)}$. Thus it is convenient to introduce local axis $\mathbf{e}_{iz'} = \mathbf{s}_i^{(0)}$ and the two perpendicular axes $\mathbf{e}_{ix'}$ and $\mathbf{e}_{iy'}$. Fixing $\mathbf{e}_{iy'}$ in the xy plane and choosing $\mathbf{e}_{ix'}$ perpendicular to both $\mathbf{e}_{iz'}$ and $\mathbf{e}_{iy'}$, one obtains

$$\mathbf{e}_{iy'} = \frac{\mathbf{s}_i^{(0)} \times \mathbf{e}_z}{|\mathbf{s}_i^{(0)} \times \mathbf{e}_z|}, \qquad \mathbf{e}_{ix'} = \mathbf{e}_{iy'} \times \mathbf{s}_i^{(0)}. \tag{11}$$

In the case $\mathbf{s}_i^{(0)} \times \mathbf{e}_z = 0$ we just choose $\mathbf{e}_{ix'} = \mathbf{e}_x$ and $\mathbf{e}_{iy'} = \mathbf{e}_y$.

Then we introduce the complex quantity

$$p_i(\omega) \equiv \delta\tilde{\mathbf{s}}_i(\omega) \cdot (\mathbf{e}_{ix'} + i\mathbf{e}_{iy'}). \tag{12}$$

Further, we introduce the real quantity

$$P_i(\omega) \equiv 2\delta\tilde{\mathbf{s}}_i(\omega) \cdot \delta\tilde{\mathbf{s}}_i^*(\omega), \tag{13}$$

that characterizes the spatial profile of spin fluctuations at the frequency ω. The function $P_i(\omega)$ has an appreciable value if the frequency ω coincides with one of the system's excitation frequencies ω_μ. If the modes are localized, $P_i(\omega)$ consists of peaks corresponding to these modes.

Another useful quantity is the projection of the excitation mode with the frequency ω on the eigenmode $\mathbf{k}$

$$Q_{\mathbf{k}}(\omega) \equiv \left(\frac{1}{N}\sum_i \delta\tilde{\mathbf{s}}_i(\omega) F_{\mathbf{k}i}\right) \cdot \left(\frac{1}{N}\sum_i \delta\tilde{\mathbf{s}}_i^*(\omega) F_{\mathbf{k}i}\right). \tag{14}$$

Especially interesting is $Q_0(\omega)$, the coupling of the mode ω to the uniform time-dependent magnetic field of such frequency. The latter is related to the absorption of microwave energy by this magnetic system. In this case one has

$$Q_0(\omega) \equiv \frac{1}{N^2} \sum_{ii'} \delta\tilde{\mathbf{s}}_i(\omega) \cdot \delta\tilde{\mathbf{s}}_{i'}^*(\omega) = \delta\tilde{\mathbf{m}}(\omega) \cdot \delta\tilde{\mathbf{m}}^*(\omega), \tag{15}$$

where $\mathbf{m}$ is the average spin (magnetization), see Eq. (4). Further,

$$\delta\tilde{\mathbf{m}}(\omega) \cdot \delta\tilde{\mathbf{m}}^*(\omega) = \frac{1}{t} \int_0^t dt' dt'' e^{i\omega(t'-t'')} \delta\mathbf{m}(t') \cdot \delta\mathbf{m}(t''). \tag{16}$$

Expressing the product $\delta\mathbf{m}(t') \cdot \delta\mathbf{m}(t'')$ through the correlation function $G(\tau)$ depending on the time difference $\tau \equiv t' - t''$, one obtains

$$Q_0(\omega) = \int_{-\infty}^{\infty} d\tau e^{i\omega\tau} G(\tau) = \tilde{G}(\omega). \tag{17}$$

The absorbed power $P_{\mathrm{abs}}(\omega)$ of the microwave radiation per spin can be expressed with the help of the fluctuation-dissipation theorem as [1]

$$\frac{P_{\mathrm{abs}}(\omega)}{h_0^2} = \frac{\omega^2 N}{12 k_B T} \tilde{G}(\omega). \tag{18}$$

III. EXPANSION OVER EXCITATION MODES

Expanding $\delta\mathbf{s}_i(t)$ over the complete set of excitation modes, one can write

$$\delta\mathbf{s}_i(t) = \sum_\mu A_{\mu i}[\mathbf{e}_{ix'}\cos(\omega_\mu t + \phi_\mu) - \mathbf{e}_{iy'}\sin(\omega_\mu t + \phi_\mu)], \tag{19}$$

where $A_{\mu i}$ is localized in space with the magnitude depending on the degree of excitation of the system. The spins are precessing clockwise in the Landau-Lifshitz equation, hence the minus sign in the second term. In RA systems, the magnetization is changing at the distances R_f, and if the modes are localized at smaller distances, the representation above should be valid.

Keeping only the slowly decaying terms with the frequency difference $\omega - \omega_\mu$ and discarding the terms with $\omega + \omega_\mu$ in Eq. (10), one obtains

$$\delta\tilde{\mathfrak{s}}_i(\omega) = \sum_\mu A_{\mu i}(\mathbf{e}_{ix'} - i\mathbf{e}_{iy'})$$
$$\times e^{i(\omega-\omega_\mu)t/2 - i\phi_\mu} \frac{\sin[(\omega-\omega_\mu)t/2]}{(\omega-\omega_\mu)\sqrt{t}}. \quad (20)$$

At large times only the terms with $t(\omega - \omega_\mu) \lesssim 1$ survive in this formula, so that the complex exponential is approximately a constant phase factor $e^{-i\phi_\mu}$. The latter depend on how the mode μ was excited and are unique for each excitation mode. One can express the function $p_i(\omega)$ in Eq. (12) in terms of the local modes as follows:

$$p_i(\omega) = \sum_\mu A_{\mu i} e^{i(\omega-\omega_\mu)t/2 - i\phi_\mu} \frac{2\sin[(\omega-\omega_\mu)t/2]}{(\omega-\omega_\mu)\sqrt{t}}. \quad (21)$$

As mentioned above, the quantity $p_i(\omega)$ is similar to the quantum wave function Ψ of the system that is a superposition of all eigenfunctions μ of a given energy $E_\mu = \hbar\omega_\mu$. One can plot $|\Psi|^2$ on the lattice that results in a system of standing waves for the pure system and peaks corresponding to local modes for the RA system. The phase of the $p_i(\omega)$ as the function of the position on the lattice i should be nearly constant in the region of a particular localized mode. For instance, looking at the correlation of the phases of two peaks close to each other, one can find out whether these peaks belong to the same or to different local modes.

Let us now calculate $P_i(\omega)$ defined by Eq. (13). Using Eq. (19) and neglecting cross terms with different values of μ and different phases, as well as fast-decaying terms with $\omega + \omega_\mu$, one obtains

$$P_i(\omega) = \sum_\mu A_{\mu i}^2 \frac{4\sin^2[(\omega-\omega_\mu)t/2]}{(\omega-\omega_\mu)^2 t}, \quad (22)$$

which is obviously related to $p_i(\omega)$ above. The terms of this expression decrease slowly in time if ω is close to ω_μ and are equal to $1/2$ for $\omega = \omega_\mu$. The quantity $P_i(\omega)$ selects all modes with frequency $\omega_\mu = \omega$. The longer the integration time t, the sharper is the selection. In the limit $t \to \infty$ the terms Eq. (22) thus become

$$P_i(\omega) = 2\pi \sum_\mu A_{\mu i}^2 \delta(\omega - \omega_\mu). \quad (23)$$

In the pure system, excitation modes' profile $P_i(\omega)$ is a superposition of standing waves. In the presence of RA, $P_i(\omega)$ consists of peaks corresponding to different localized modes. Numerical calculations indeed show the behavior $P_i(\omega) \propto 1/t$.

For $Q_0(\omega)$ defined by Eq. (15), using the representation of spin deviations in terms of local modes, Eq. (19), one can use

$$\delta\mathbf{m}(t) = \frac{1}{N}\sum_{\mu i} A_{\mu i}[\mathbf{e}_{ix'}\cos(\omega_\mu t + \phi_\mu) - \mathbf{e}_{iy'}\sin(\omega_\mu t + \phi_\mu)]. \quad (24)$$

Discarding cross terms with $\mu \neq \mu'$ and assuming $\mathbf{e}_{i''x'} \cdot \mathbf{e}_{i''x'} \cong \mathbf{e}_{i'y'} \cdot \mathbf{e}_{i''y'} \cong 1$ and $\mathbf{e}_{i'x'} \cdot \mathbf{e}_{i''y'} \cong \mathbf{e}_{i'y'} \cdot \mathbf{e}_{i''x'} \cong 0$, one obtains

$$Q_0(\omega) = \frac{1}{t}\int_0^t dt' dt'' e^{i\omega(t'-t'')} \frac{1}{N^2}\sum_\mu \bar{A}_\mu^2 \cos[\omega_\mu(t'-t'')], \quad (25)$$

where

$$\bar{A}_\mu \equiv \sum_i A_{\mu i} \quad (26)$$

is the spatial average of the excitation-mode amplitude. One can see that only modes with a nonzero spatial average contribute to the power absorption as they couple to the uniform time-dependent external field. Integrating over the difference time in Eq. (25) as above, one obtains

$$Q_0(\omega) = \frac{1}{N^2}\sum_\mu \bar{A}_\mu^2 \int_{-t'} d\tau e^{i\omega\tau}\cos(\omega_\mu\tau). \quad (27)$$

At large times this becomes

$$Q_0(\omega) = \frac{\pi}{2}\frac{1}{N^2}\sum_\mu \bar{A}_\mu^2 \delta(\omega - \omega_\mu). \quad (28)$$

Comparing this with Eq. (17), one obtains the Fourier transform of the time correlation function of the magnetization as

$$\tilde{G}(\omega) = Q_0(\omega) = \frac{\pi}{2}\frac{1}{N^2}\sum_\mu \bar{A}_\mu^2 \delta(\omega - \omega_\mu). \quad (29)$$

This quantity defines the absorbed power given by Eq. (18).

A. Characterization of the localized modes

One of the quantities characterizing excitation modes is the average peak width δ of the landscape of $P_i \equiv P_{n_x n_y}$. To estimate it, one can use two different methods. The first method is more pedestrian and directly computes the averaged half-width of the peaks at their average half-height. To find the average height of the peaks, we partitioned the system into 10×10 blocks, found the maximal values of $P_{n_x n_y}$ in each block and then averaged these values. Then the total number of sites having the height exceeding the half of the maximal height was computed. The result, in lattice units, is the area of all peaks $A_p = N_p \pi \delta^2$, where N_p is the number of peaks and δ is the peak width at the half-height. Computing the number of peaks N_p is a separate problem. One cannot just find all maxima of the function $P_{n_x n_y}$ because in a random system there are lots of minor peaks on the slope of a major peak. Taking all them into account leads to a strong underestimation of the average peak width that should be defined by the major peaks only. The solution is to consider the islands of $P_{n_x n_y}$ that are above the half of the average peak height B as major peaks. Counting the number of these islands is a standard problem of

connected-component labeling that arises, in particular, in image recognition. So, we used one of the available algorithms to compute N_p, after which we found $\delta = \sqrt{A_p/(\pi N_p)}$.

Another method is more sophisticated and uses summation of different powers m and n of $P_{n_x n_y}$ to extract the peaks' height and the area of all peaks. It is assumed that $P_{n_x n_y}$ is a collection of Gaussian peaks $f(r) = B \exp(-r^2/\delta^2)$, Lorentzian peaks $f(r) = B/(1 + r^2/\delta^2)$, or any bell-like functions. Assuming that there are N_p such nonoverlapping peaks, one can define

$$W_m \equiv \int_0^\infty d^2 r f^m(r) dr = N_p B^m \delta^2 q_m, \qquad (30)$$

where q_m is a number: $q_m = \pi/m$ for the Gaussian function and $q_m = \pi/(m-1)$ for the Lorentzian function. One can see that W_m depends on the peak height B and the area of all peaks $A_p = N_p \pi \delta^2$. For the Lorentzian function, δ is exactly the half-width at the half-height of the peak, thus we will use this function in interpreting the results. Having two such integrals for different values of m allows us to find the peaks' height B and the area of all peaks A_p as

$$B = \left(\frac{\widetilde{W}_m}{\widetilde{W}_n}\right)^{1/(m-n)}, \qquad A_p = \pi \frac{\widetilde{W}_n^{m/(m-n)}}{\widetilde{W}_m^{n/(m-n)}}, \qquad (31)$$

where $\widetilde{W}_m \equiv W_m/q_m$ etc. Applying this to the problem at hand, one computes $W_m = \sum_{n_x n_y} P_{n_x n_y}^m$ and $W_n = \sum_{n_x n_y} P_{n_x n_y}^n$ from which one finds the average peak height and peaks' area using the formulas above. The powers m and n have to be larger than one to ensure the convergence at large distances from the peaks and to suppress the contribution of the low-level noise background. To find the number of peaks, one computes the number of islands in which $P_{n_x n_y} > B/2$ with the help of the same connected-component labeling routine. Then the peak width is defined as above, $\delta = \sqrt{A_p/(\pi N_p)}$. As the shape of the peaks is unknown, the first and simpler method of measuring the peaks' width is preferable. The second method is used only to check the consistency of the results.

One more parameter characterizing localization is based on symmetry. Increasing randomness leads to the transformation of symmetric patterns of standing waves in $P(\omega)$, see Figs. 1 and 2 to random patterns typical for localized excitations, see Fig. 3. Here we try to find computable quantities allowing us to trace the transition from extended to localized states. One idea is that symmetric patterns can be reduced by antisymmetrization with respect to the center of the system while asymmetric patterns cannot. Using the compound index $i = (n_x, n_y)$ in the square lattice, for $P_{n_x,n_y}(\omega)$ with $n_x = 1, 2, \ldots, N_x$ and $n_y = 1, 2, \ldots, N_y$ one can define

$$\widetilde{P}_{n_x,n_y} \equiv \left| P_{n_x,n_y} - P_{N_x-n_x,n_y} \right|. \qquad (32)$$

For a symmetric pattern, $\widetilde{P}_{n_x,n_y}$ will be zero, while for a collection of random peaks it nearly doubles. Further, one can define

$$\widetilde{\widetilde{P}}_{n_x,n_y} \equiv \frac{1}{2} \left| \widetilde{P}_{n_x,n_y} - \widetilde{P}_{n_x,N_y-i_y} \right| \qquad (33)$$
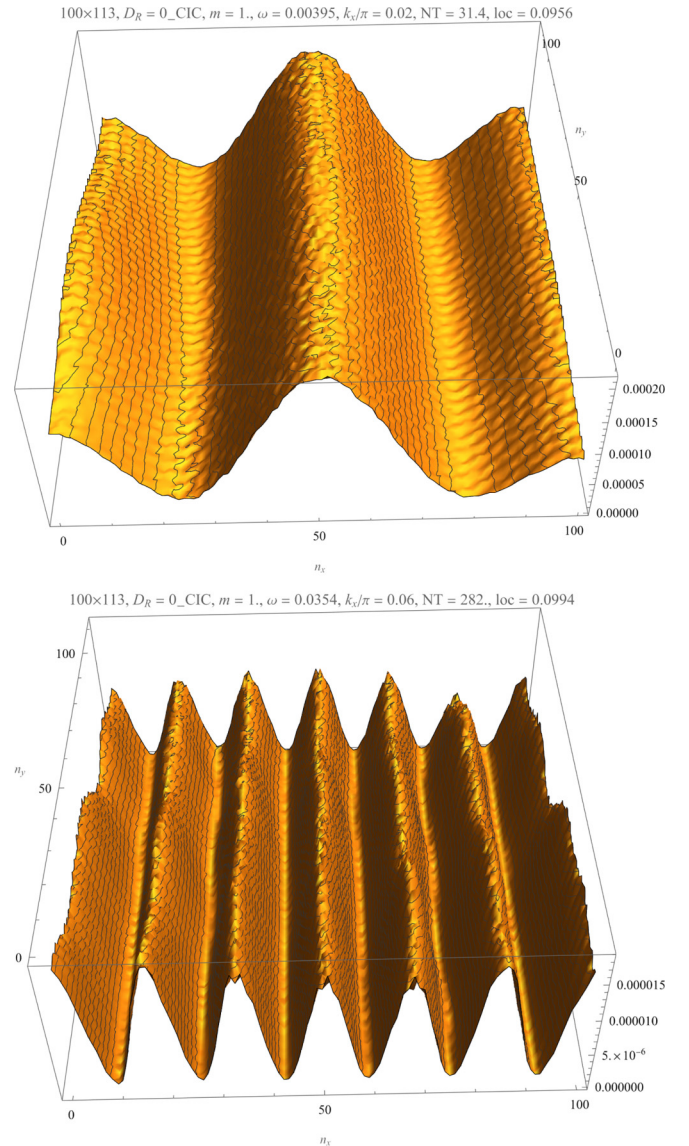

FIG. 1. Spatial profiles of spin fluctuations $P_i(\omega)$, Eq. (13), in the pure 100×113 system at $H = 0$ and $T/J = 0.01$ at different frequencies matching those of spin-wave modes, Eq. (9). Top: $k_x/\pi = 0.02$. Bottom: $k_x/\pi = 0.06$.

to further reduce the pattern and define the localization parameter

$$\zeta = \sum_{n_x,n_y} \widetilde{\widetilde{P}}_{n_x,n_y} \Big/ \sum_{n_x,n_y} P_{n_x,n_y} \qquad (34)$$

that changes between nearly zero for $D_R = 0$ (symmetric excitation patterns) and nearly two for $D_R \sim J$ (rarified local-mode peaks). In fact, it is better to use the minimal value of the quantity defined above and that with reflection of i_y and then of i_x.

B. Localization and power absorption

Localization of excitation modes in a magnetic system leads to power absorption in a broad range of frequencies.
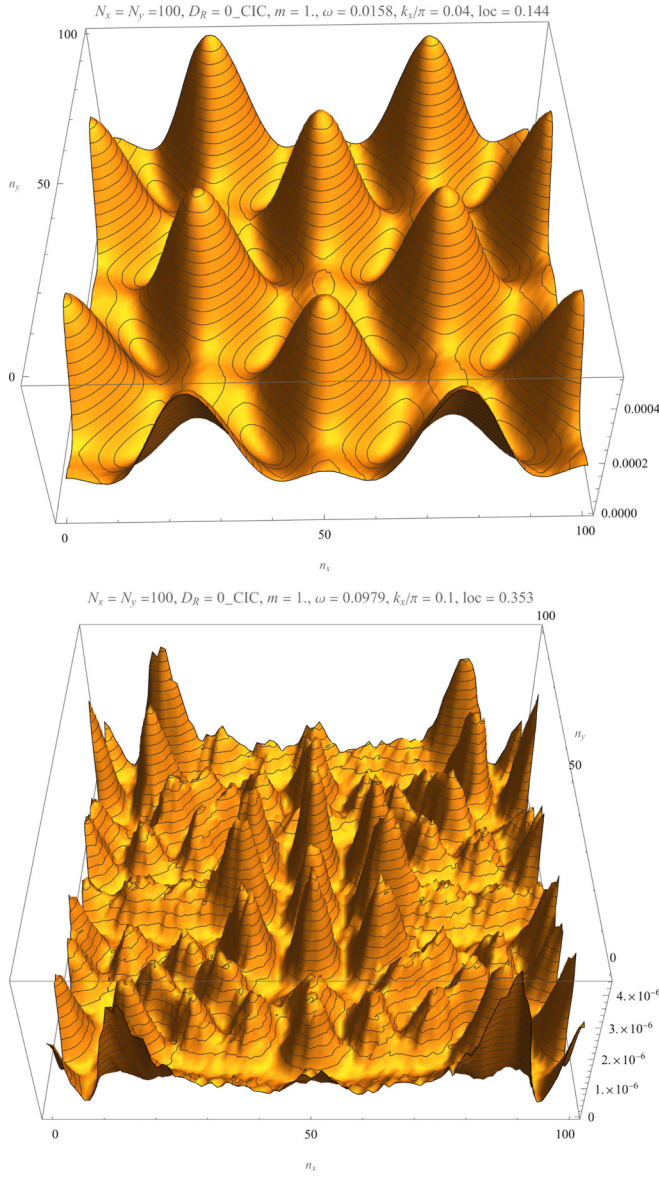
FIG. 2. Spatial profiles of spin fluctuations $P_i(\omega)$, Eq. (13), in the pure system at $H = 0$ and $T/J = 0.01$ at different frequencies matching those of spin-wave modes. Top: $k/\pi = 0.04$. Bottom: $k/\pi = 0.1$.

FIG. 3. Normalized spatial profiles of spin fluctuations $P_i(\omega)$, Eq. (13), in the 200×2130 RA system with $D_R/J = 0.3$ (top) and $D_R/J = 1$ (bottom) at $H = 0$ and $T/J = 0.01$ at one of the frequencies matching those of spin-wave modes, Eq. (9): $\hbar\omega/J = 0.0354$ corresponding to $k/\pi = 0.06$.

In a pure system, there is the uniform mode that is the only mode coupled to the microwave field that has $\mathbf{k} = \mathbf{0}$. All other eigenmodes of the system are orthogonal to the uniform mode and thus they cannot absorb microwave energy. Random anisotropy breaks translational invariance of the system, thus plane waves, including the uniform mode, are no longer eigenmodes. Actual eigenmodes all have a nonzero projection on the uniform mode and thus they are coupled to the microwave field and can absorb its energy. A sufficiently strong RA leads to localization of excitation modes that are described by the peaks of $P_i(\omega)$, as shown, e.g., in Fig. 3. The integrals over the localized eigenmode amplitudes $\bar{A}_\mu$ in Eq. (26) that enter the Fourier transform of the time correlation function of magnetization components, $\tilde{G}(\omega)$, are, in general, nonzero and can be estimated via the peak parameters introduced in
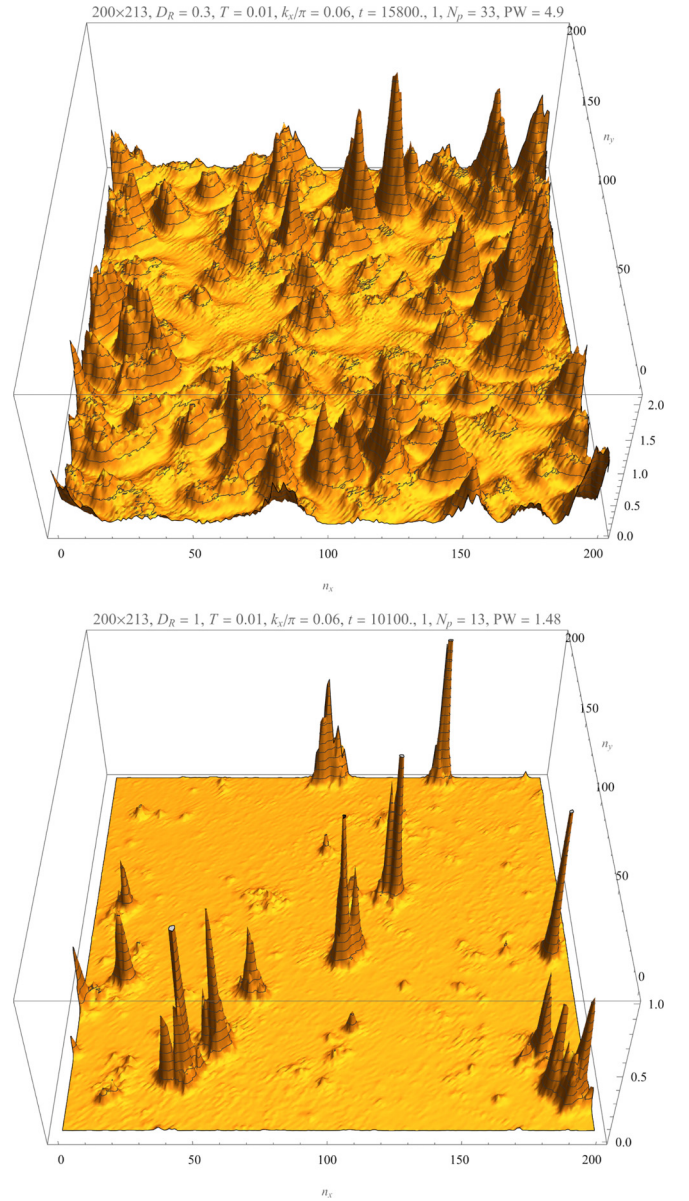
Sec. III A. As an estimation, one can use

$$\bar{A}_{\mu^2} \equiv \left(\sum_i A_{\mu i}\right)^2 \sim \delta^2 \sum_i A_{\mu i}^2, \qquad (35)$$

where δ is the average peak width in lattice units. This allows one to relate $Q_0(\omega)$ in Eq. (28) with $P_i(\omega)$ in Eq. (23) and obtain

$$\tilde{G}(\omega) = Q_0(\omega) \sim \frac{\delta^2}{N^2} \sum_i P_i(\omega) \qquad (36)$$

for $\tilde{G}(\omega)$ that enters the formula for the microwave absorption, Eq. (18). The sum in this formula does not depend on the time

and scales with the system size N, so that $\tilde{G}(\omega) \propto 1/N$. This ensures that the absorbed power per spin in Eq. (18) does not depend on the system size. Further, one can relate the power absorption to the average peaks height B and the number of peaks N_p using Eqs. (30) and (31) with $m = 1$. This yields $\sum_i P_i(\omega) \sim B\delta^2 N_p$ that results in

$$\tilde{G}(\omega) \sim \frac{N_p}{N^2} B\delta^4. \tag{37}$$

After that the absorbed power, Eq. (18), becomes

$$\frac{P_{\text{abs}}(\omega)}{h_0^2} = \frac{\omega^2 N}{12 k_B T} \tilde{G}(\omega) = \frac{N_p}{N} \frac{\omega^2 B \delta^4}{12 k_B T}. \tag{38}$$

One can see that power absorption depends on the peak width δ, the ratio of the peak height to the temperature B/T, and peaks' concentration N_p/N, all at the frequency ω.

IV. NUMERICAL RESULTS FOR THE LOCALIZED MODES

Numerical calculations were performed with Wolfram *Mathematica* using compilation and parallelization. The system sizes studied ranged from 10^4–10^6 spins. Computations for different values of D_R were done in parallel. We used three different computers with 8, 8, and 16 cores.

A. Visualization of excitation modes

Figure 1 shows spatial profiles of spin fluctuations $P_i(\omega)$, Eq. (13), in the pure 100×113 system at $H = 0$ and $T/J = 0.01$ at two different frequencies matching those of spin-wave modes, Eq. (9). As expected, these profile are close to the squares of the spin-wave eigenfunctions, Eq. (7), for the corresponding k. In the system of square shape there is a degeneracy of SW modes with $\mathbf{k}$ along the 10 and 01 directions in the lattice. Thus spin fluctuations can contain superpositions of the corresponding SW eigenstates with the weights depending on the state after thermalization. This can lead to checkered patterns of the spatial profiles of spin fluctuations, as shown in Fig. 2. In particular, in the top panel this is the square of the antisymmetric superposition of the two states in Eq. (6), $F_{k,n_x n_y}^2 = (f_{n_x k} - f_{n_y k})^2$. In the bottom panel there is apparently a superposition of a larger number of modes.

Figure 3 shows spatial profiles of spin fluctuations $P_i(\omega)$, Eq. (13), in the RA system with $D_R/J = 1$ at $H = 0$ and $T/J = 0.01$ at two different frequencies matching those of spin-wave modes, Eq. (9). Here, unlike the results for the pure model shown in Fig. 1, spatial spin profiles are irregular and localized, which implies localization of spin waves in the presence of randomness. This effect was detected in Ref. [26] by exciting the 2D RA magnet by short (five periods) pumping by a weak time-dependent magnetic field at particular frequencies (see Fig. 11). The response to the pumping was localized in space as narrow peaks that oscillated in time. Here local modes are investigated more accurately by making a Fourier transform of thermal spin fluctuations over long times. At such times, the spatial profiles stabilize and only peaks oscillating with the frequency close to the frequency set in the Fourier transformation are selected.

In contrast to the standing waves in pure model, the excitation modes in the RA system are apparently localized. The
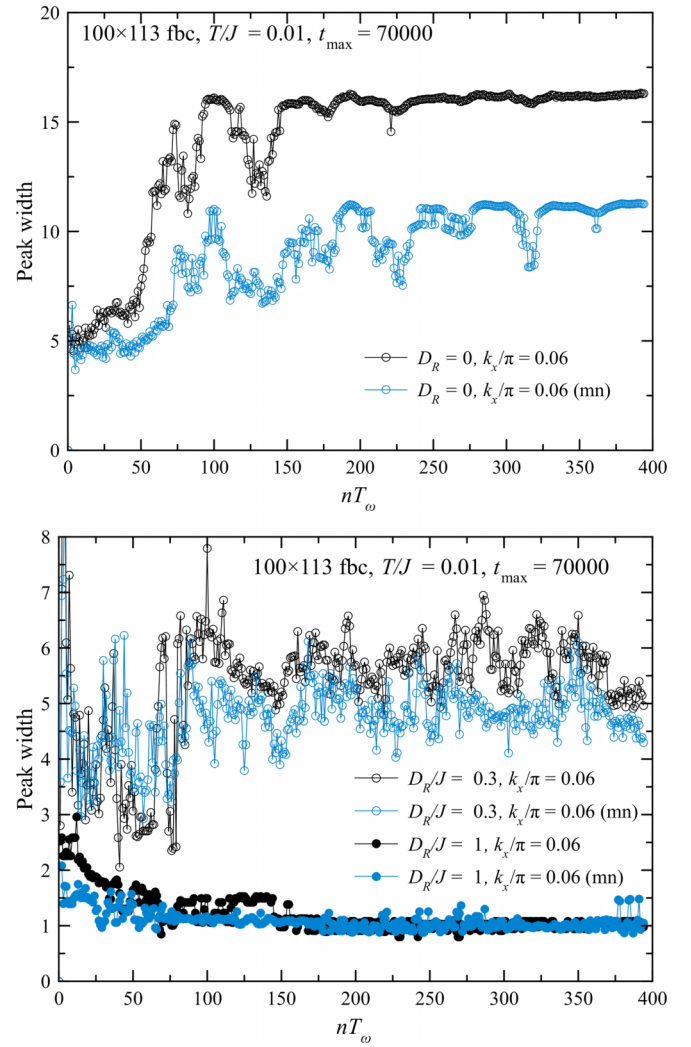

FIG. 4. The average peak width vs the number of periods of the mode frequency corresponding to the pure $k_x/\pi = 0.06$ mode measured by two methods. Results obtained by the second method are labeled with "(mn)". Top: Pure system, $D_R = 0$. Bottom: $D_R/J = 0.3$ and 1.

shape and positions of the peaks are irregular. Also, the peaks are rarified. This can be explained by the redistribution of the density of states. In the pure model, $P_i(\omega)$ has an appreciable value if ω matches one of the quantized spin-wave frequencies $\omega_\mathbf{k}$ and a very small value otherwise. In the random model with $D_R/J \sim 1$, one can expect that the frequencies of the modes are not quantized and take any values in a particular range.

B. Investigation of the localized modes parameters

The results for the average peak width vs the integration time up to $t = 70000$ in Eq. (10) in periods of the frequency corresponding to the $k_x/\pi = 0.06$ mode in the pure system, obtained by the two methods, are shown in Fig. 4. The curves in the top panel for the pure system show gradual selection of the standing wave along the x axis of the type shown in Fig. 1. A significant difference between the peak widths computed by the two methods is due to the washboard profile with no peaks
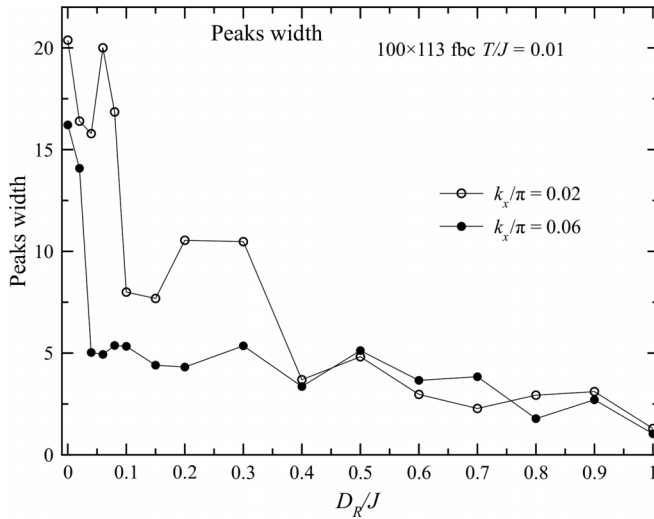
FIG. 5. The average peak width δ vs D_R/J for a system of the size 100×113 and the frequencies corresponding to the pure $k_x/\pi = 0.02$ and 0.06 modes.

FIG. 6. Localization parameter ζ vs D_R/J for a system of the size 100×113 and the frequencies corresponding to the pure $k_x/\pi = 0.02$ and 0.06 modes.

in this case. In the presence of RA in the bottom panel, the results obtained by the two methods are in a good accordance. The results do not significantly change with the evolution time and there are significant fluctuations that do not die out with the time [see comments below Eq. (22)].

For larger system sizes, the spin-wave modes becomes densely spaced, so that there are modes with many different **k** having nearly the same frequency. This makes selection of only one mode, as in Fig. 1, impossible. Instead, one obtains a complicated landscape with many peaks due to the superposition of many different standing waves.

The results for the average peak width at the end of the evolution obtained with the first method are shown in Fig. 5. One can see that the peaks become narrower for larger D_R. The scatter is rather large for this moderate system size.

The results for symmetry localization parameter ζ for the system of 100×113 spins with FBC obtained by the solution of the equation of motion within the time interval $t_{max} = 50000$, see Eq. (10), are shown in Fig. 6. The data scatter is large for this moderate system size. The results below were obtained from the same computation of the evolution of the thermal spin state.

Numerical results for our largest system of 10^6 spins, 1000×1013 are shown in Figs. 7 and 8. The first figure shows the dependences of both the average peaks' width δ and peaks' concentration N_p/N on D_R at different frequencies ω. Both quantities decrease with D_R and weakly depend on ω in the frequency range under investigation. These results for the peaks' width are in accord with those for our small system, 100×113, in Fig. 5. The results for the symmetry localization parameter ζ in Fig. 8 differ from those in Fig. 6 as ζ approaches one rather than zero in the pure limit. This can be explained by the large amount of different modes with frequencies ω_μ close to ω a the large system. Superposition of these modes with random phases does not possess a clear symmetry that is needed to render $\zeta = 0$. As in the pure limit excitation modes are delocalized, the peaks of $P_i(\omega)$ are broad is no empty space between them. For this reason, symmetry
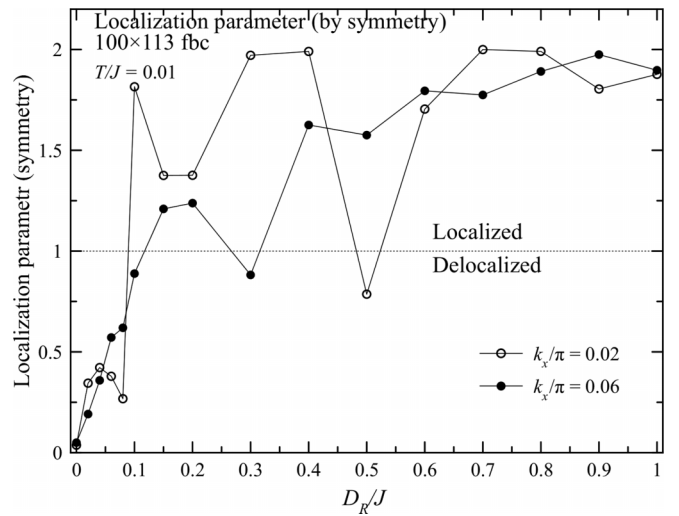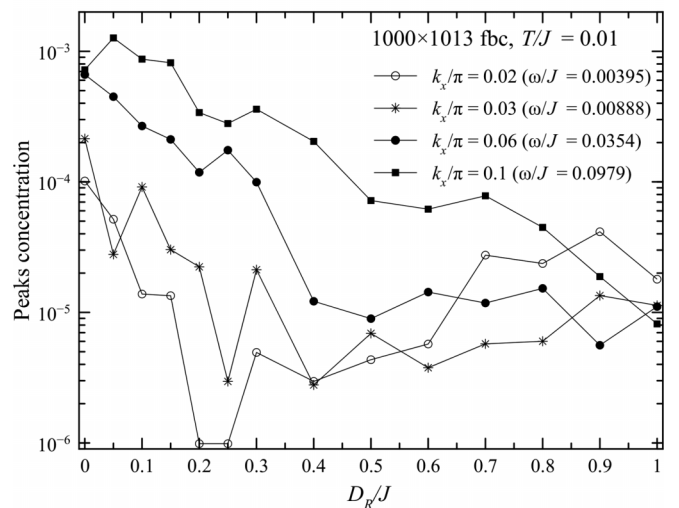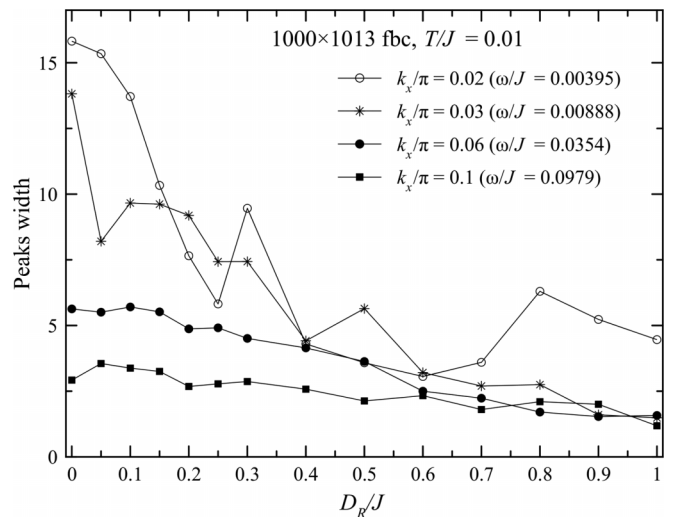

FIG. 7. Average peaks' widths δ (top) and peaks' concentration N_p (bottom) vs the RA strength D_R at different frequencies for the 1000×1013 system.
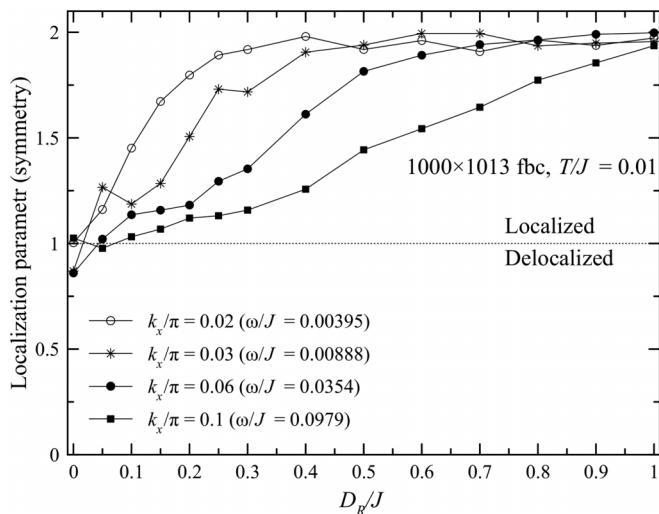
FIG. 8. Localization parameter ζ vs D_R/J at different frequencies for a system of the size 1000×1013.

operations above result in annihilation and creation of peaks at the same rate that yields $\zeta = 1$. With increasing D_R, peaks become rarified, so that they do not overlap with annihilation as the result of symmetry operations, and the number of peaks doubles, leading to $\zeta = 2$.

C. Investigation of the modes' phases

In this section, we investigate the phase effect in the dynamics of the excitation modes of a RA magnet by computing and plotting the phase of the function $p_i(\omega)$ defined by Eq. (12). For the pure model, $D_R = 0$, there is a system of standing waves that possesses extended phase correlations of the type shown in Fig. 9. Here the phase is represented as a 3D plot with color coding by by the Hue[$\phi/(2\pi)$] function. The phase is bound to the interval $(-\pi, \pi)$, thus the argument of the Hue function is in the $(-0/5, 0.5)$ interval. At the end of this interval, the cyan color is output, and within this interval, there are all rainbow colors. For the pure system, the phase is plotted everywhere. For the RA system with localized modes, the mode intensity $P_i(\omega)$ is small outside the peaks, and in these regions the phase is not well defined. Thus for the RA system the phase is plotted only in the peaks' regions.

Excitation-mode peaks of $P_i(\omega)$ situated at some distance from each other can be independent local modes or they can be parts of the same mode. The distinguishing between these cases is subtle and depends on the coupling between the close mode peaks. The question of the latter can be investigated with the help of Eq. (21) by computing the phase of $p_i(\omega)$. The numerical experiment is the following. For one realization of the random anisotropy, one finds a local energy minimum. Then one performs parallelized Monte Carlo thermalization cycles at a very low temperature (here $T/J = 0.01$) for a number of replicas of the system (for instance, equal to the number of processor cores). Each of these computations leads to different thermal states with different degrees of excitation of each mode and their different phases. After that, parallelized computation of the system's dynamical evolution is run and $p_i(\omega)$ are computed for each replica. If the phase
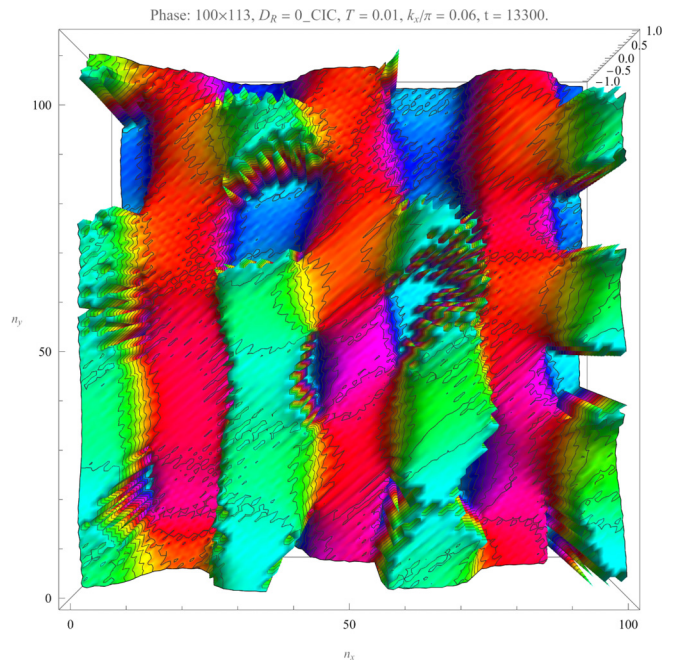

FIG. 9. A typical phase landscape of a system of standing spin waves in a pure ($D_R = 0$) 100×113 system color coded by the Hue function.

relation between different mode peaks is the same for different replicas, these peaks belong to the same mode, otherwise, they are independent local modes.

An example of the output of this procedure is shown in Fig. 10. In the top and bottom panels, for the 100×113 system with $D_R/J = 0.3$ the peaks shown by geodesic lines are combined with the phase at some moment of time, color coded by the Hue function as explained above. The two panels are picked out of eight ones resulting from the parallelized computation. (All eight panels can be seen in the Supplemental Material [32].) One can see peaks having the same phases having the same or nearly the same color and labeled by the same number: 1, 2, or 3. For the two different panels, the phases are different, as it should be given the random nature of the excitation of modes by Monte Carlo. But the phases are the same within the groups. Thus one can conclude that the two peaks labeled by 1 belong the same mode and, most likely, the peak between them also belongs to the same mode. Apart from this, peaks labeled by 2 and by 3 must belong to the same excitation mode. Likewise, as groups of peaks 2 and 3 are interceded, they are likely parts of the same extended mode. To conclude, for $D_R/J = 0.3$ there is a system of standing waves distorted by RA rather than independent localized modes.

In contrast, for $D_R/J = 1$ peaks are narrow and rarified, see bottom panel of Fig. 3, so that the interaction between them should be negligible and each peak should correspond to an individual local mode.

V. LOCALIZATION LENGTH VIA EDGE PUMPING

The study of the thermal dynamics of the RA magnet above includes a characterization of the excitation modes that allows
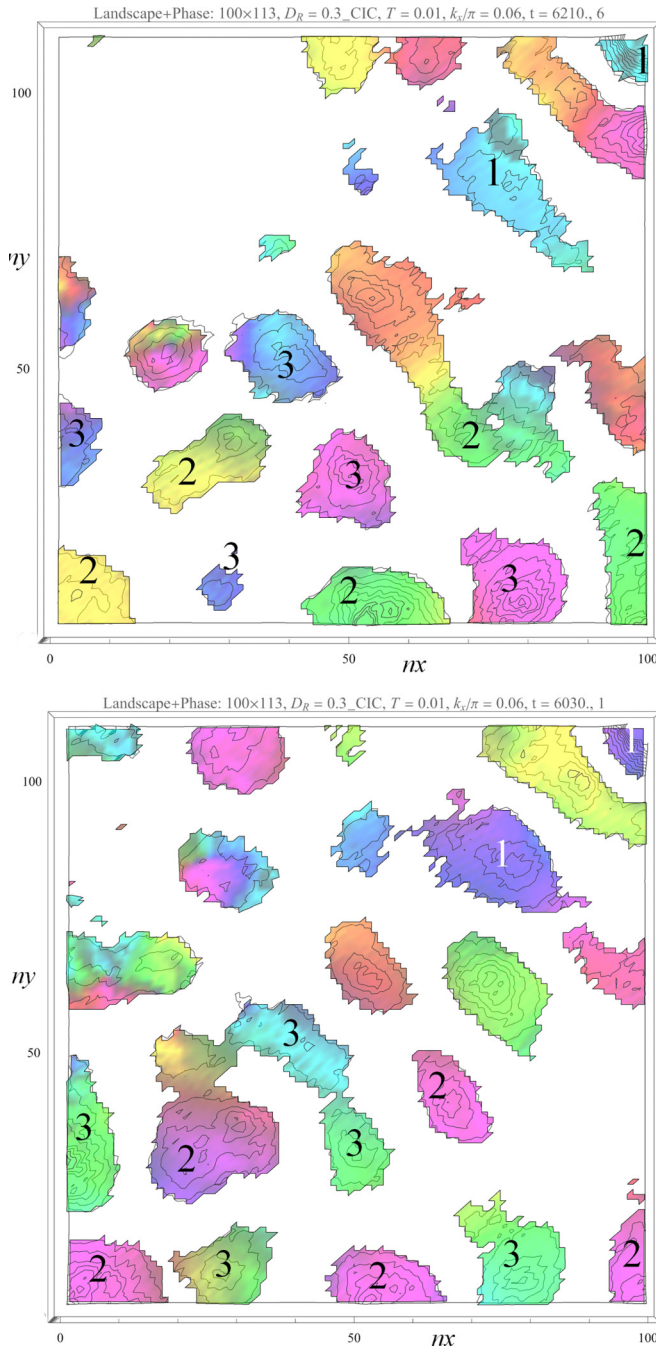
FIG. 10. Excitation-mode peaks with their phases marked by colors. The top and bottom panels have the same RA configuration and the same local-energy-minimum state, however, they have undergone different Monte Carlo procedures to excite the modes that as the result have different phases. Peaks labeled by the same color and the same number are in-phase and thus belong to the same excitation mode.

us to judge if they are extended or localized. However, this characterization does not prove that the modes are indeed localized. Many peaks resonating at the same frequency may be different localized modes or they can be the same mode with several peaks. The latter happens if local modes become hybridized by the interaction or, as it can be put, there is tunneling between degenerate or quasidegenerate local modes.

The localization can be tested, for instance, by the edge-pumping method. A sinusoidal magnetic field at a frequency ω_0 matching that of one of standing waves is applied to the spins at one of the boundaries and it is monitored how the excitation is penetrating into the body of the system. For the pure system, a standing wave of the matching frequency is excited. In the case of localized modes in the strong-RA model, the wave is not penetrating into the body of the system and excitation is limited to the region near the pumped edge. This experiment allows us to estimate the localization length. If the left boundary, $n_x = 1$, is pumped, one can define the excitation profile

$$P_{n_x}(\omega) = \delta\bar{\mathbf{s}}_{n_x}(\omega) \cdot \delta\bar{\mathbf{s}}_{n_x}^*(\omega), \tag{39}$$

where $\delta\bar{\mathbf{s}}_{n_x}(\omega)$ is the average over the transverse direction:

$$\delta\bar{\mathbf{s}}_{n_x}(\omega) \equiv \frac{1}{N_y} \sum_{n_y=1}^{N_y} \delta\tilde{\mathbf{s}}_{n_x,n_y}(\omega), \tag{40}$$

whereas $\delta\tilde{\mathbf{s}}_{n_x,n_y}(\omega) \equiv \delta\tilde{\mathbf{s}}_i(\omega)$ is given by Eq. (10). The localization length, in lattice units, can be estimated as

$$\xi_{\text{loc}} = \frac{1}{P_1(\omega)} \sum_{n_x=1}^{N_x} P_{n_x}(\omega). \tag{41}$$

For the pure system it is close to $N_x/2$ but decreases with increasing D_R. It turns out that regions inside the system may respond stronger to pumping than the left boundary because these local modes are at resonance with the pumping whereas the left-boundary region is not. However, choosing a very large N_y one can average these effects out. Still, even at large N_y, the response $\delta\tilde{\mathbf{s}}_{n_x}(\omega)$ for small D_R/J can be larger somewhere away from the boundary. To deal with this, it is better to replace $P_1(\omega) \Rightarrow \max(P_{n_x}(\omega))$ in the definition of ξ_{loc}.

As an illustration, the edge-pumping excitation profiles for the 50×5013 RA model at the frequency corresponding to the pure-system standing wave with $k_0/\pi = 0.06$ are shown in Fig. 11. Here, for $D_R/J \leqslant 0.3$ the wave is weakly damped and penetrates into the whole system. Notice that for $D_R/J = 0.2$ the maximum at $n_x \simeq 15$ is higher than the value at $n_x = 1$, thus it make sense to use this value for the normalization instead of $P_1(\omega)$ in Eq. (41).

The dependence of the localization length on D_R is shown in Fig. 12 for systems of different sizes and the same frequency corresponding to $k_0/\pi = 0.06$. Whereas for small D_R the result depends on the system length N_x as expected, for stronger RA all points merge to a size-independent curve indicating the localization. As, especially for large N_x, it takes some time to form a standing wave, pumping should last for a number of periods N_{T_0} of the pumping frequency. In Fig. 12 we used $N_{T_0} = 10$. The fitted dependence of the localization length is $\xi_{\text{loc}} = 4.1(J/D_R)^{3/2}$. This differs from the dependence $R_f \propto J/D_R$ that follows from Eq. (5) in two dimensions.

The dependence of the computed localization length ξ_{loc} on the number of periods of pumping n_{T_0} up to $n_{T_0} = 30$ is shown in Fig. 13. One can see that the values of ξ_{loc} asymptotically saturate but for smaller D_R it takes a longer time. For $D_R/J = 1$, the asymptotic value is reached immediately as the excitation mode is strongly localized. One result for $N_{T_0} = 30$
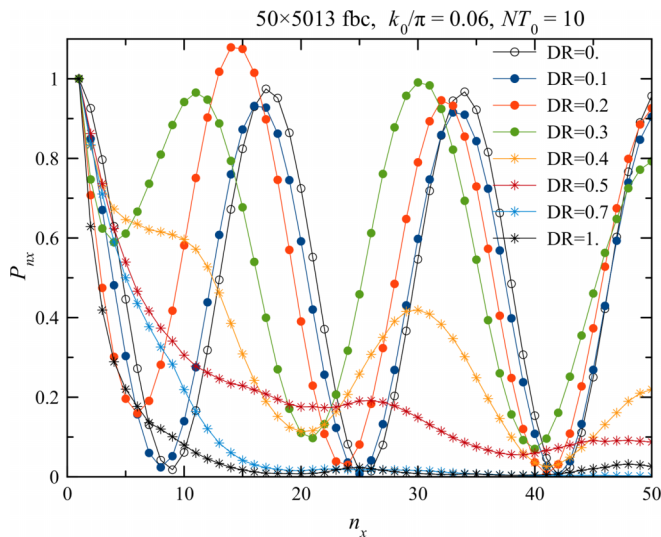
FIG. 11. The edge-pumping excitation profiles, normalized by their value at the left boundary, for the 50×5013 RA model at the frequency corresponding to the pure-system standing wave with $k_0/\pi = 0.06$. The localization effect becomes strong for $D_R/J = 0.4$.

is shown in Fig. 12 but the difference with the $N_{T_0} = 10$ result is nonessential.

The numerical results show that the localization length ξ_{loc} is independent of the pumping frequency within the numerical scatter. It is close to the peak width computed from the dynamics of the thermally excited state, see Fig. 5. The latter also does not depend on the frequency. Thus we conclude that there is a sufficient evidence of the localization of excitation modes in the RA model.

There has to be a relation between the localization of spin waves and the spin-wave damping. The time decrement Γ (relaxation rate) should be related to the spatial decrement κ by the same relation as frequency and wave vector, that is, $\Gamma_k = v_k \kappa$, where v is the spin-wave group velocity $v_k = d\omega_k/dk$.
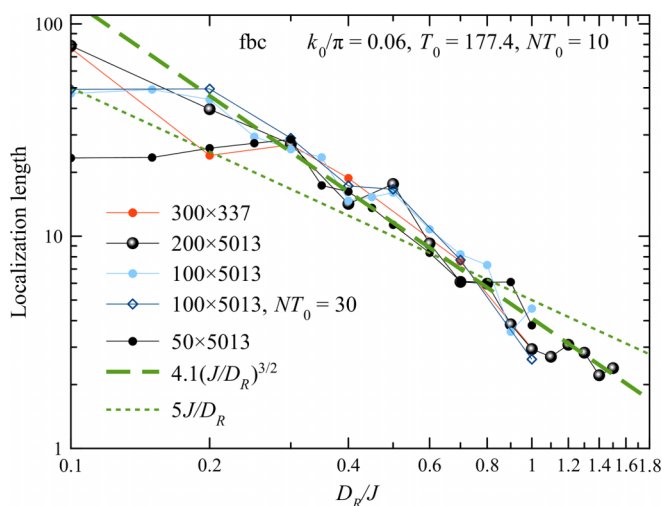

FIG. 12. Localization length ξ_{loc} vs D_R/J for systems of different sizes at the frequency corresponding to $k_0/\pi = 0.06$.
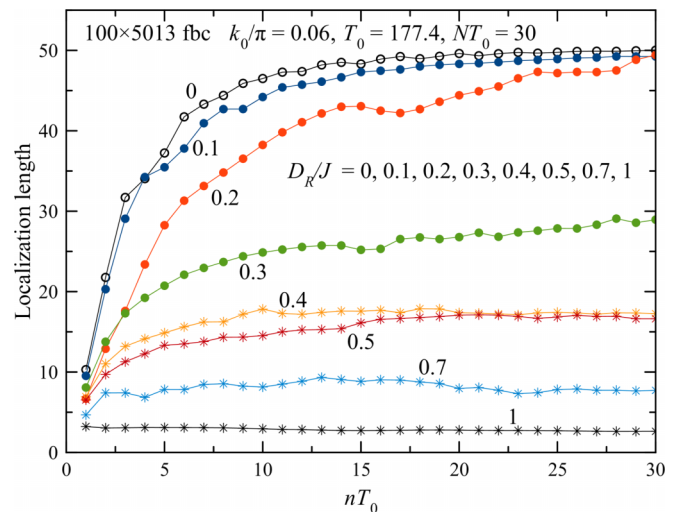

FIG. 13. The dependence of the computed localization length ξ_{loc} on the number of periods of pumping n_{T_0} for the 100×5013 system.

From Eq. (9) in the long-wavelength limit one obtains $\hbar\omega_{\mathbf{k}} = 4J(ak)^2$ and thus $v_k = 8(J/\hbar)a^2k$. With $\kappa = 1/\xi_{\text{loc}}$ one obtains $\Gamma_k = 8(J/\hbar)a^2k/\xi_{\text{loc}}$. If ξ_{loc} does not depend on k, then $\Gamma_k \propto k$.

VI. CONCLUSION

We have studied localized spin excitations in an RA magnet. Our main results can be summarized as follows. Standing spin waves in a finite-size sample evolve into localized modes on increasing the strength of the RA. We visualized this process by taking snapshots of spin oscillations in a 2D system. The study of phases of localized excitations shows that they generally consist of a group of well-separated peaks oscillating coherently. The average width of the peak, which we identify with the localization length, decreases on increasing the strength of the RA, scaling roughly as $(J/D_R)^{3/2}$.

Notice that in the absence of topological defects, the ferromagnetic correlation length in a 2D RA magnet scales as J/D_R. However, in a 2D Heisenberg model with three-component spins, the effect of topological defects (skyrmions in particular) must be significant [24]. It must lead to the decay of ferromagnetic correlations on a shorter scale that is consistent with the $(J/D_R)^{3/2}$ dependence on the RA strength and the suggestion [26] that localized excitations in the RA magnets are hosted by the Imry-Ma domains.

Broad distribution on the effective magnetic anisotropy for Imry-Ma domains is responsible for the broad distribution of spin-precession frequencies in the RA magnets. Combined with the high density of the Imry-Ma domains, it provides strong broadband absorption of microwave power. The width of the band rapidly increases on increasing the strength of the RA. Our studies of the excitation of localized modes by the ac magnetic field establish a connection between localization and power absorption.

Based upon dissipation-fluctuation theorem, one can show that the integral power absorption in an RA magnet, $\int_{-\infty}^{\infty} d\omega P(\omega)$, is proportional to D_R^2. Combined with the dependence of the localization length on D_R shown in Figs. 5,

7, 12, it indicates that the integral power scales inversely with the localization length. Earlier we demonstrated [26] that the height of the peak in $P(\omega)$ has a weak dependence on the RA strength. This makes the integral power a measure of the absorption bandwidth. The results obtained in this paper show that the broadband absorption of microwaves by random magnets is intimately related to the localization of spin excitations: The stronger the localization the greater the bandwidth.

It would be interesting to visualize the localization of spin oscillations in an amorphous or sintered ferromagnetic film in a real experiment that would generate images similar to the ones shown in Fig. 3. This could be done by, e.g., covering the film with a fluorescent layer that reacts to the inhomogeneous absorption of microwave power by the magnetic layer.

[1] D. A. Garanin and E. M. Chudnovsky, Random anisotropy magnet at finite temperature, J. Phys.: Condens. Matter **34**, 285801 (2022).

[2] A. I. Larkin, Effect of inhomogeneities on the structure of the mixed state of superconductors, Sov. Phys. JETP **31**, 784 (1970).

[3] Y. Imry and S.-k. Ma, Random-Field Instability of the Ordered State of Continuous Symmetry, Phys. Rev. Lett. **35**, 1399 (1975).

[4] W. M. Saslow and C. Sun, Longitudinal resonance for thin film ferromagnets with random anisotropy, Phys. Rev. B **98**, 214415 (2018).

[5] R. Bruinsma and S. N. Coppersmith, Anderson localization and breakdown of hydrodynamics in random ferromagnets, Phys. Rev. B **33**, 6541(R) (1986).

[6] R. A. Serota, Spin-wave localization in ferromagnets with weak random anisotropy, Phys. Rev. B **37**, 9901(R) (1988).

[7] M. Ma, B. I. Halperin, and P. A. Lee, Strongly disordered superfluids: Quantum fluctuations and critical behavior, Phys. Rev. B **34**, 3136 (1986).

[8] L. Zhang, Disordered boson systems: A perturbative study, Phys. Rev. B **47**, 14364 (1993).

[9] J. P. Álvarez Zúñiga and N. Laflorencie, Bose-Glass Transition and Spin-Wave Localization for 2D Bosons in a Random Potential, Phys. Rev. Lett. **111**, 160403 (2013).

[10] X. Yu and M. Müller, Localization of disordered bosons and magnets in random fields, Ann. Phys. (NY) **337**, 55 (2013).

[11] M. Evers, C. A. Müller, and U. Nowak, Spin-wave localization in disordered magnets, Phys. Rev. B **92**, 014411 (2015).

[12] V. S. Amaral, B. Barbara, J. B. Sousa, and J. Filippi, Spin-wave localization in random anisotropy systems: Amorphous $(Dy_xGd_{1-x})Ni$, Europhys. Lett. **22**, 139 (1993).

[13] S. Suran and E. Boumaiz, Longitudinal resonance in ferromagnets with random anisotropy: A formal experimental demonstration, J. Appl. Phys. **81**, 4060 (1997).

[14] G. Suran, Z. Frait, and E. Boumaz, Direct observation of the longitudinal resonance mode in ferromagnets with random anisotropy, Phys. Rev. B **55**, 11076 (1997).

[15] S. Suran and E. Boumaiz, Longitudinal-transverse resonance and localization related to the random anisotropy in a-CoTbZr films, J. Appl. Phys. **83**, 6679 (1998).

[16] R. D. McMichael, D. J. Twisselmann, and A. Kunz, Localized Ferromagnetic Resonance in Inhomogeneous Thin Film, Phys. Rev. Lett. **90**, 227601 (2003).

[17] G. de Loubens, V. V. Naletov, O. Klein, J. Ben Youssef, F. Boust, and N. Vukadinovic, Magnetic Resonance Studies of the Fundamental Spin-Wave Modes in Individual Submicron Cu/NiFe/Cu Perpendicularly Magnetized Disks, Phys. Rev. Lett. **98**, 127601 (2007).

[18] C. Du, R. Adur, H. Wang, S. A. Manuilov, F. Yang, D. V. Pelekhov, and P. C. Hammel, Experimental and numerical understanding of localized spin wave mode behavior in broadly tunable spatially complex magnetic configurations, Phys. Rev. B **90**, 214428 (2014).

[19] E. M. Chudnovsky, W. M. Saslow, and R. A. Serota, Ordering in ferromagnets with random anisotropy, Phys. Rev. B **33**, 251 (1986).

[20] E. M. Chudnovsky and J. Tejada, *Lectures on Magnetism* (Rinton Press, Princeton, 2006).

[21] T. C. Proctor, E. M. Chudnovsky, and D. A. Garanin, Scaling of coercivity in a 3d random anisotropy model, J. Magn. Magn. Mater. **384**, 181 (2015).

[22] E. M. Chudnovsky, Random anisotropy in amorphous alloys, in *Magnetism of Amorphous Metals and Alloys*, edited by J. A. Fernandez-Baca and W.-Y. Ching (World Scientific, Singapore, 1995), Chap. 3, pp. 143–174.

[23] P. Marin and A. Hernando, Applications of amorphous and nanocrystalline magnetic materials, J. Magn. Magn. Mater. **215–216**, 729 (2020).

[24] T. C. Proctor, D. A. Garanin, and E. M. Chudnovsky, Random Fields, Topology, and the Imry-Ma Argument, Phys. Rev. Lett. **112**, 097201 (2014).

[25] X. Zeng, X. Cheng, R. Yu, and G. D. Stucky, Electromagnetic microwave absorption theory and recent achievement in microwave absorbers, Carbon **168**, 606 (2020).

[26] D. A. Garanin and E. M. Chudnovsky, Absorption of microwaves by random-anisotropy magnets, Phys. Rev. B **103**, 214414 (2021).

[27] E. Akkermans and G. Montambaux, *Mesoscopic Physics of Electrons and Photons* (Cambridge University Press, Cambridge, 2007).

[28] D. A. Garanin, E. M. Chudnovsky, and T. C. Proctor, Random field xy model in three dimensions, Phys. Rev. B **88**, 224418 (2013).

[29] D. A. Garanin, Energy balance and energy correction in dynamics of classical spin systems, Phys. Rev. E **104**, 055306 (2021).

[30] D. A. Garanin, Pulse-noise approach for classical spin systems, Phys. Rev. E **95**, 013306 (2017).

[31] H. Kachkachi and D. A. Garanin, Boundary and finite-size effects in small magnetic systems, Physica A **300**, 487 (2001).

[32] See Supplemental Material at http://link.aps.org/supplemental/10.1103/PhysRevB.107.134411 for eight figures showing

excitation-mode peaks with their phases marked by colors. They all have the same RA configuration and the same local-energy-minimum state. However, they have undergone different Monte Carlo procedures to excite the modes that as the result have different phases. Peaks labeled by the same color are in phase and thus belong to the same excitation mode. Fig. 10 shows only two of these figures.